Magnetic Field Mapper
Using Commercial off the Shelf (COTS) Components

Yubo Fu*, Filippo Di Benedetto*, Devin Kelsey*, Andrew Orr*, Ezra Keto*, and Álvaro Romero-Calvo†
Georgia Institute of Technology, Atlanta, Georgia, 30332, United States

Novel applications of magnetism are the focus of multiple research efforts, in a diverse set of disciplines, including aerospace technologies. Due to the inherent material variations in hysteresis-producing coils and other factors, manufacturing errors in permanent magnets are expected. Thus, investigations involving magnetic materials often require independent field characterization. Although commercial measuring equipment is available for this purpose, the precision expected of such instruments imposes an outsize cost, creating a significant financial obstacle to research on magnetism. This paper documents a cost-effective solution to magnetic flux density mapping using commercially available components. The system employs a Hall-effect sensor mounted on a 3D printer, interfaced utilizing a combination of open-source and in-house software. Results indicate the system is capable of field characterization with a mean error and standard deviation of less than 1 mT relative to numerical results with a spatial resolution of 0.1 mm and for a total system cost under 2,200 USD (FY-2024).

I. Introduction

Many engineering projects require precise and accurate knowledge of the magnetic flux density of a given magnetic component beyond standard datasheet values. This need becomes critical for systems utilizing complex shapes or magnetic structures like Halbach arrays [1]. Such applications include but are not limited to, adaptive liquid optics [2], control of particle beams [3], nuclear magnetic resonance spectroscopy [4], calibration of magnetic instruments [5], design and manufacturing of brushless motors [6], magnetohydrodynamic fluid control [7], or magnetic propellant positioning [8, 9].

The fundamental behavior of permanent magnets has been well understood for over a century [10], and simulations based on Maxwell's equations regularly enable theoretical analysis of complex field arrangements. However, these tools implement assumptions on the uniformity of the magnetic material that may deviate from reality to a degree significant enough to impact its end application. Magnetization is not a static property; the magnetization of permanent magnets can be significantly affected by temperature [11] and mechanical stress [12]. Deviations in magnetization between magnets of the same size and material are expected, and in some cases, they have been known to influence the behavior of systems utilizing permanent magnets [13]. Consequently, characterization methods for the exact magnetic flux density (commonly referred to as the B-field) in three-dimensional space are necessary for many applications.

Commercial magnetic characterization systems are accurate, with typical measurement error at or below 0.1% and micrometer position accuracy. However, these systems tend to be cost-prohibitive; an integrated 3D mapping platform may require an investment of over 100,000 USD*. Thus, a replicable, open-source, magnetic field mapping platform constructed using easy-to-obtain components would greatly improve the accessibility of magnet characterization. There exist multiple published projects with a similar scope. However, previous implementations of this concept require custom-manufactured components [14, 15], are designed for a particular type of scan or application [16], are limited to field measurements in one axis [17], or otherwise require construction that is more technically involved than the procedures described here [18]. In contrast, this project solely utilizes commercial-off-the-shelf (COTS) components or hardware that may be additively manufactured using only the requisite 3D printer, which exemplifies the focus on ease of implementation and use.

The mapping system consists of two primary components: a 3D printer used as a Cartesian translation frame, and a 3-axis Hall effect magnetic field sensor. A serial connection is established between both components and a personal computer. To conduct a field characterization scan, the provided software commands the frame to a point of interest, where the sensor collects and averages a predetermined set of measurements for each field component. This process is

*Undergraduate Research Assistant, Daniel Guggenheim School of Aerospace Engineering, AIAA Undergraduate Members
†Assistant Professor, Daniel Guggenheim School of Aerospace Engineering, AIAA Member 978289, alvaro.romerocalvo@gatech.edu
*Accuracy and cost figures retrieved from `https://gmw.com/product/magnetic-field-mapper`

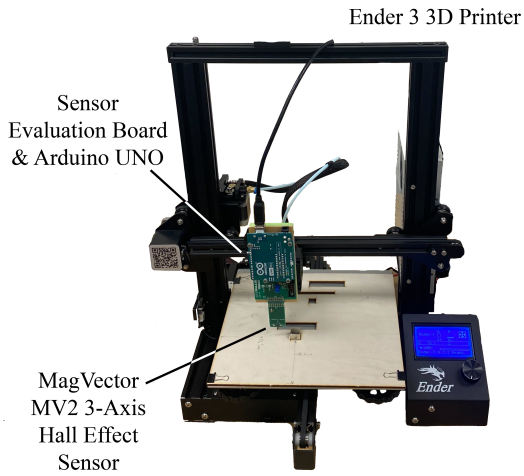

Fig. 1 Magnetic field mapper assembly

repeated for all points of interest, generating a complete scan of the magnetic flux density in the desired area surrounding the component. In this paper, Sec. II presents the methods with which this instrument is constructed and operated. The results, validation, and example applications are provided in Sec. III.

II. Methods

A. Overview

The mapping frame, sensor, and other hardware are available commercially or through design files accessible through the provided GitHub repository located at `https://github.com/LGST-LAB/mag_mapper` under the GNU GPL 3.0 license. The frame, a Creality Ender 3 3D printer, translates the sensor throughout the space surrounding the component under study. The chosen sensor is a Metrolab MagVector MV2 3-axis Hall Effect magnetometer. The sensor is mounted to the frame using a custom mount manufactured solely using the 3D printer. The sensor is attached to this mount using standard metric hardware. Interfacing between a personal computer and the sensor is accomplished with the MV2 Evaluation Kit, an accessory board provided with the sensor that enables serial communication using an Arduino UNO R3.

The user interface, translation commands, and data compilation are handled by a custom LabVIEW environment. Data acquisition and processing are controlled by a script onboard the Arduino UNO, provided by Metrolab.

B. Printing Platform

The Creality Ender 3 is an introductory level 3D printer with a print area of 220 x 220 x 250 mm and a spatial resolution of 0.1 mm. As a common open-source hobby-grade 3D-printing platform, a plethora of documentation, tools, and 3rd-party extensions are available. This allows for simple customization to fit the project's parameters and desire for replicability. The system utilizes the open-source Marlin Instrument Driver[†], developed by Jón Schone of *Proper Printing*, to send and receive commands and buffer from the printer via serial port.

C. Field Sensor

The MagVector MV2 3-axis Hall effect sensor is a highly capable commercial magnetometer. With a sensitivity of 3.75 μT and selectable B-field ranges from 0.1 to 30 T[‡], the sensor's performance enables an accurate field characterization. The implementation discussed in this work uses the sensor in its analog mode.

[†]Available under a Creative Commons license at `https://properprinting.pro/product/marlin-instrument-drivers-for-labview/`

[‡]Sensor specifications available at `https://www.metrolab.com/wp-content/uploads/2020/06/MagVector-MV2-Datasheet-v2.5.pdf`

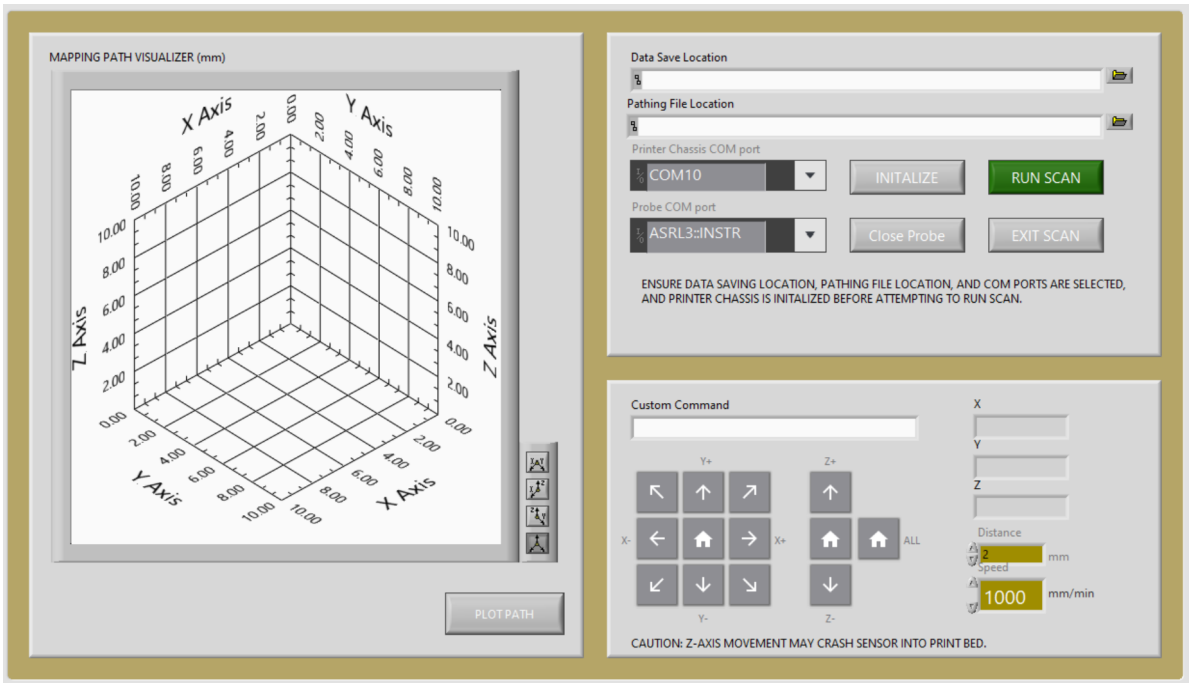

Fig. 2 The Labview GUI provided to interact with the mapping system.

D. Interfacing and Data Flow

LABVIEW is selected as the main interfacing software for its ability to easily create graphical user interfaces and script complex procedures for the simultaneous operation of multiple serial devices. The interface communicates via G-code with the 3D printer and continuously reads and records magnetometer data.

The LabVIEW environment front panel, shown in Fig. 2 consists of 3 main sections. The top right consists of an input section asking to specify COM ports, end the program, and provide user input files. A .csv file is used to specify the path, allowing users to easily create custom pathing files and have the LabVIEW program handle conversion to G-code. The leftmost panel previews the scan path specified, while the lower right panel is a movement controller.

The mapping program data flow is summarized in Fig. 3. The magnetic field scanning function begins with LabVIEW reading a comma-separated value file containing an array of 3D spatial points generated by the user. An example pathing algorithm implemented in MATLAB is provided. The program converts the coordinates specified in the pathing file to G-code and sends the command to the printer. The interface then commands the system to wait until each movement is complete before continuing. Following each movement, a short pause occurs to eliminate the influence of mechanical vibration, after which LabVIEW begins recording the magnetometer data for n number of trials, which can be customized within the LabVIEW program. The sensor position, B-field data, mean and standard deviation for each trial are calculated and continuously written to a text file, preventing data losses from external events such as a loss of power. An excerpt from an output file is provided in Listing 1.

Listing 1 Excerpt of an output file.

```
X,          Y,          Z,          Bx,         By,         Bz
140.500000, 137.500000, 51.500000, −22.793442, 19.427800, 25.226428
141.500000, 137.500000, 51.500000, −25.153484, 22.335892, 25.009603
142.500000, 137.500000, 51.500000, −27.635335, 26.250887, 24.141515
143.500000, 137.500000, 51.500000, −30.995224, 29.296799, 22.829256
144.500000, 137.500000, 51.500000, −32.241223, 31.277195, 20.964304
145.500000, 137.500000, 51.500000, −34.266296, 33.898822, 18.464223
146.500000, 137.500000, 51.500000, −36.078197, 36.216612, 15.417234
147.500000, 137.500000, 51.500000, −37.456158, 38.179777, 12.014331
```

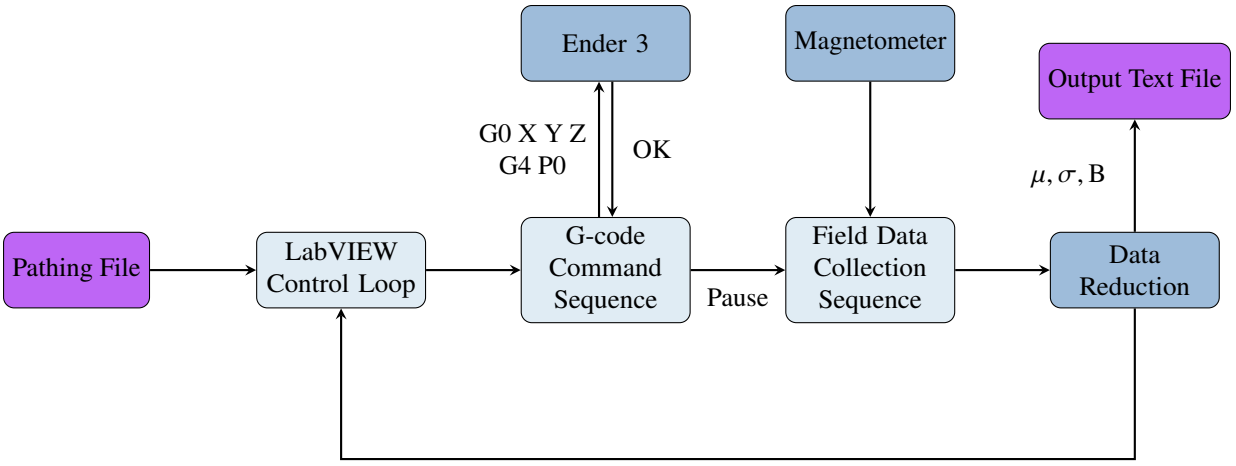

Fig. 3 Flowchart of the Mapping Sequence Commands.

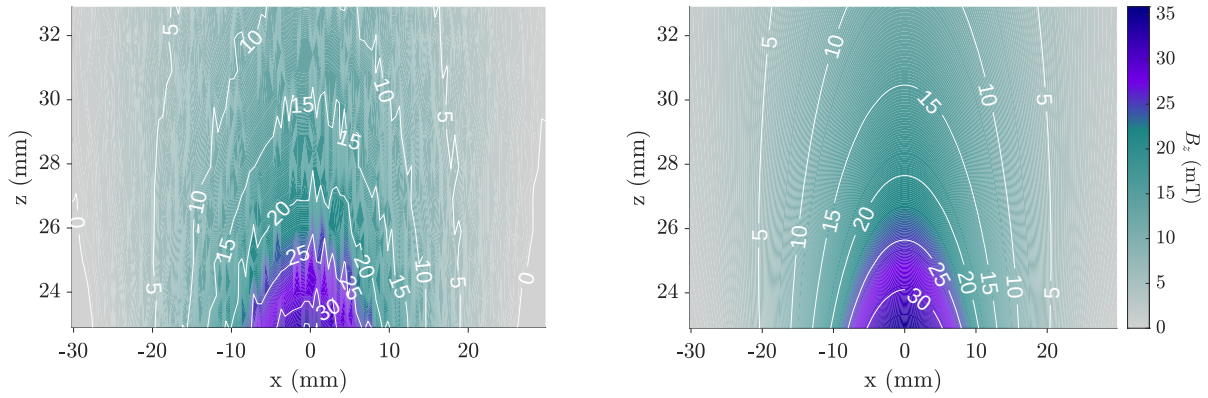

(a) Measured B_z. **(b) Simulated B_z.**

Fig. 4 Measured and simulated B_z above a 1/2" N52 cube magnet following calibration procedure.

E. Calibration

To accurately align the component position in the mapping frame coordinate system, a calibration routine is conducted using a 1/2" N52 cube magnet. The center position of the component is first measured manually. A rough scan is taken of the component with low spatial resolution and only 10 measurements per point. The estimated magnet position from this scan is then adjusted to align with a simulated magnet with the same size and properties. Results from an example calibration routine are shown in Fig. 4.

F. Simulation

To validate the sensor, simulation results are generated by approximating a cubic permanent magnet as four surface currents $\boldsymbol{K}_m = \boldsymbol{M}_m \times \boldsymbol{n}$ in the lateral walls, where $\boldsymbol{M}_m$ is the magnetization and $\boldsymbol{n}$ is the normal vector to each surface. The magnetic vector potential from each surface can then be calculated as [19]

$$\boldsymbol{A}(r) = \frac{\mu_0}{4\pi} \oint_S \frac{\boldsymbol{K}_m(\boldsymbol{r}')}{|\boldsymbol{r} - \boldsymbol{r}'|} da', \tag{1}$$

where μ_0 is the permeability of free space, $\boldsymbol{r}'$ is the position of an infinitesimal point on the surface, $\boldsymbol{r}$ is the position of interest, and a is an infinitesimal area on the surface. The flux density $\boldsymbol{B}$ can be calculated as

$$\boldsymbol{B} = \nabla \times \boldsymbol{A}. \tag{2}$$

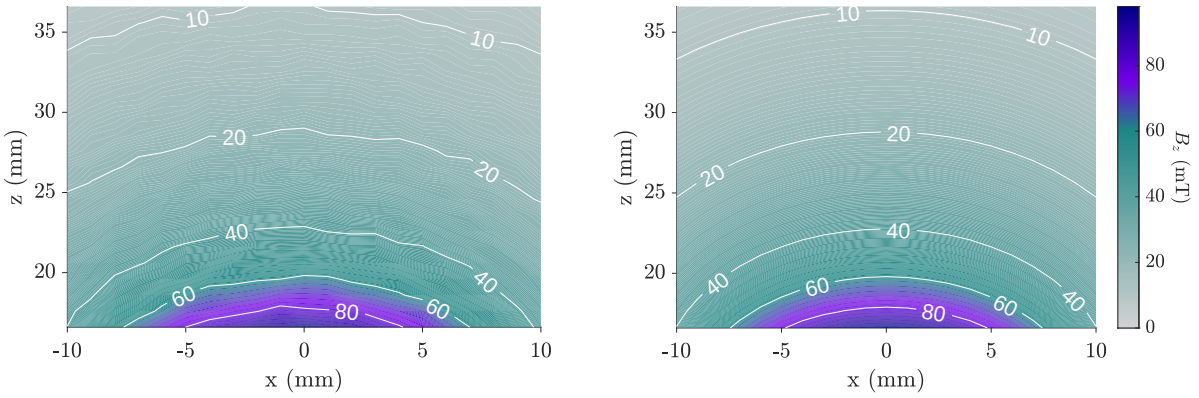

(a) Measured B_z. **(b) Simulated B_z.**

Fig. 5 Measured and simulated B_z above a 1/2" N52 cube magnet.

The contributions from each surface are superimposed to generate the field at a given point. This process is then repeated for each point of interest.

III. Results and Discussion

Measurements from 1/2" and 3/16" N52 cube magnets and simulations with identical parameters are shown in Fig. 5 and 6. Simulated fields are generated using the procedure described in Sec. II.F. The distribution of percent error throughout the scan space for each test is shown in Fig. 7. Table 1 provides a full error analysis for each test. Both validation tests include 30 measurements per point.

Results indicate the system can successfully measure the flux density field throughout 3D space. Both tests generate a mean error and standard deviation under 1 mT for all field components relative to identical simulated magnets. The error distribution indicates percent error is concentrated primarily where the field is very small, and is otherwise evenly distributed. Although general agreement with theoretical expectations is demonstrated, these results indicate the system is not yet on the order of accuracy of a commercial mapping system. Field variations are beyond those expected from any commercial-grade permanent magnet, and display a 'jittery' quality, particularly as the field magnitude decreases.

Primary sources of error likely include uncertainty in the position of the magnet in the printer coordinate system and noise generated during the analog-to-digital conversion conducted by the Arduino board. Other potential sources of error include undesired fields generated by magnetized objects or currents, inaccuracies in printer motion, and mechanical vibrations in the printer frame. Performance gains may be realized through many potential system improvements. A robust system or revised method for determining component position could eliminate uncertainty regarding unaligned reference frames. Furthermore, tuning or modification of the printer's movement system may assist with alignment. Noise in the sensor output could be reduced through the implementation of the sensor's digital mode. Replacement of the printer's metallic build plate or other magnetizable components could further reduce error.

A 3D view of two orthogonal measurement planes is provided in Fig. 8. This perspective highlights the full capability and utility of the system as a fully three-dimensional mapping platform.

Table 1 Error analysis for both 1/2" N52 and 3/16" N52 scans at 30 measurements per point. Mean error and standard deviation are calculated over scan points for each field component.

	1/2" N52 cube			3/16" N52 cube		
	B_x	B_y	B_z	B_x	B_y	B_z
Mean percent error	0.1%	4.4%	2.7%	2.7%	4.5%	4.6%
Mean error (mT)	0.2741	0.5844	0.4985	0.9497	0.1975	0.4264
Standard deviation (mT)	0.4867	0.5981	0.5375	0.543	0.1898	0.5658

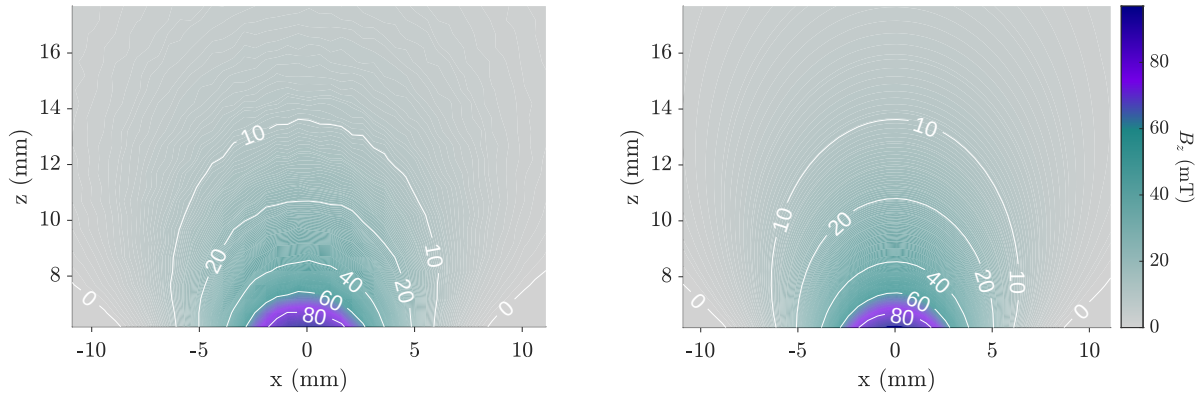

(a) Measured B_z. **(b) Simulated B_z.**

Fig. 6 Measured and simulated B_z above a 3/16" N52 cube magnet.

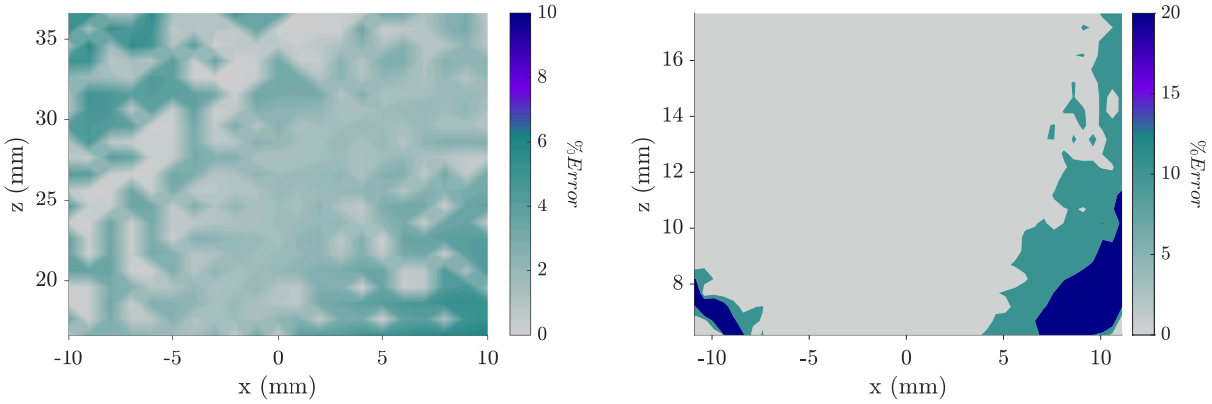

(a) Percent error distribution of the B_z component relative to simulated values above a 1/2" cube N52 magnet. **(b) Percent error distribution of the B_z component relative to simulated values above a 3/16" N52 cube magnet.**

Fig. 7 Error distribution for both scans above permanent magnets.

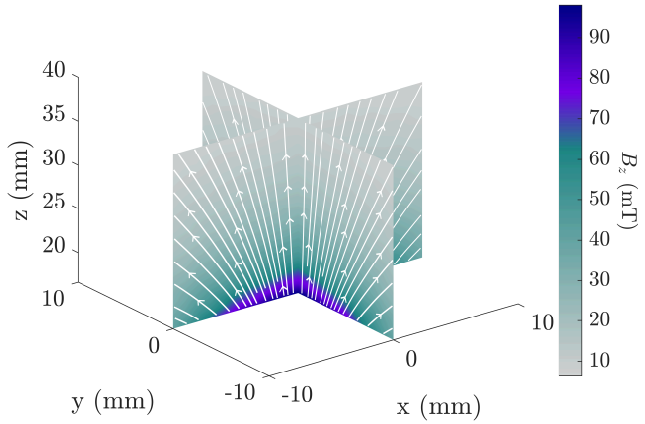

Fig. 8 3D view of measurements taken of a 1/2" N52 cube magnet in two orthogonal slice planes, including field lines.

IV. Conclusion

The magnetic mapping system presented here combines readily available COTS components into an accessible device. Demonstrating acceptable accuracy against simulation results to 1 mT, for a total system cost below 2,200 USD, this instrument displays potential as an accessible magnetic mapping approach. The documentation for the construction and operation of this platform is publicly available under the GNU GPL 3.0 license at `https://github.com/LGST-LAB/mag_mapper`.

Acknowledgments

The authors thank Amy Ritter, Irene Abraham, Devindi Ambawatta, Zoe Robertson, Jessica Ly, Zhen-Yin Lee, and Brice Shearwood for their contributions to this project, Tianyang Hu for the simulation software utilized in this work, Sam Hart for assistance reviewing this work, and Shay Vitale for his mentorship. The authors also thank the Georgia Space Grant Consortium for their financial support, enabling the presentation of this paper.

References

[1] Halbach, K., "Application of permanent magnets in accelerators and electron storage rings," *Journal of Applied Physics*, Vol. 57, No. 8, 1985, pp. 3605–3608. https://doi.org/10.1063/1.335021.

[2] Laird, P. R., Bergamasco, R., Berube, V., Borra, E. F., Gingras, J., Ritcey, A.-M. R., Rioux, M., Robitaille, N., Thibault, S., Vieira da Silva, L., Jr., and Yockell-Lelievre, H., "Ferrofluid-based deformable mirrors: a new approach to adaptive optics using liquid mirrors," *Adaptive Optical System Technologies II*, edited by P. L. Wizinowich and D. Bonaccini, SPIE, 2003. https://doi.org/10.1117/12.459065.

[3] Miao, C.-H., Liu, M., Yin, C.-X., and Zhao, Z.-T., *Nuclear Science and Techniques*, Vol. 28, No. 172, 2017. https://doi.org/10.1007/s41365-017-0324-6.

[4] Marion, D., "An introduction to biological NMR spectroscopy," *Mol Cell Proteomics*, Vol. 12, No. 11, 2013, pp. 3006–3025. https://doi.org/10.1074/mcp.O113.030239.

[5] Belsten, N., Knapp, M., Masterson, R., Payne, C., Ammons, K., Lind, F. D., and Cahoy, K., "Verification and calibration of a commercial anisotropic magnetoresistive magnetometer by multivariate non-linear regression," *Geoscientific Instrumentation, Methods and Data Systems*, Vol. 12, No. 2, 2023, pp. 201–213. https://doi.org/10.5194/gi-12-201-2023.

[6] Praveen, R. P., Ravichandran, M. H., Sadasivan Achari, V. T., Jagathy Raj, V. P., Madhu, G., and Bindu, G. R., "A Novel Slotless Halbach-Array Permanent-Magnet Brushless DC Motor for Spacecraft Applications," *IEEE Transactions on Industrial Electronics*, Vol. 59, No. 9, 2012, pp. 3553–3560. https://doi.org/10.1109/TIE.2011.2161058.

[7] Romero-Calvo, A., Schaub, H., and Cano-Gómez, G., "Diamagnetically Enhanced Electrolysis and Phase Separation in Low Gravity," *Journal of Spacecraft and Rockets*, Vol. 59, No. 1, 2022, pp. 59–72. https://doi.org/10.2514/1.A35021.

[8] Romero-Calvo, , Maggi, F., and Schaub, H., "Magnetic Positive Positioning: Toward the application in space propulsion," *Acta Astronautica*, Vol. 187, 2021, pp. 348–361. https://doi.org/https://doi.org/10.1016/j.actaastro.2021.06.045.

[9] Hart, S. T., Lightsey, E. G., and Álvaro Romero-Calvo, "Thermoelectromagnetic SmallSat propellant positioning," *Acta Astronautica*, Vol. 214, 2024, pp. 427–438. https://doi.org/https://doi.org/10.1016/j.actaastro.2023.11.007.

[10] Maxwell, J. C., "VIII. A dynamical theory of the electromagnetic field," *Philosophical Transactions of the Royal Society of London*, Vol. 155, 1865, pp. 459–512. https://doi.org/10.1098/rstl.1865.0008.

[11] Ohring, M., *Engineering Materials Science*, Academic Press, San Diego, 1995. https://doi.org/10.1016/B978-0-12-524995-9.X5023-5.

[12] Hauser, H., and Fulmek, P., "The effect of mechanical stress on the magnetization curves of Ni- and FeSi-single crystals at strong fields," *IEEE Transactions on Magnetics*, Vol. 28, No. 3, 1992, pp. 1815–1825. https://doi.org/10.1109/20.141291.

[13] Jaeger, M., Drichel, P., Schröder, M., Berroth, J., Jacobs, G., and Hameyer, K., "On magnetization deviations as the dominant cause for vibration harmonics in the spectrum of a PMSM drive," *Archives of Electrical Engineering*, Vol. 70, No. 3, 2021, pp. 719–730. https://doi.org/10.24425/aee.2021.137584.

[14] Nasir, M., Shoaib, M., Hassan, M. U., and Anwar, M. S., "Design and implementation of a versatile magnetic field mapper for 3D volumes," *HardwareX*, Vol. 12, 2022, p. e00356. https://doi.org/https://doi.org/10.1016/j.ohx.2022.e00356.

[15] Han, H., Moritz, R., Oberacker, E., Waiczies, H., Niendorf, T., and Winter, L., "Open Source 3D Multipurpose Measurement System with Submillimetre Fidelity and First Application in Magnetic Resonance," *Scientific Reports*, Vol. 7, No. 13452, 2017. https://doi.org/10.1038/s41598-017-13824-z.

[16] Vavoulas, A., Vaiopoulos, N., Hedström, E., Xanthis, C. G., Sandalidis, H. G., and Aletras, A. H., "Using a modified 3D-printer for mapping the magnetic field of RF coils designed for fetal and neonatal imaging," *Journal of Magnetic Resonance*, Vol. 269, 2016, pp. 146–151. https://doi.org/https://doi.org/10.1016/j.jmr.2016.06.005.

[17] Omelyanchik, A., Marqués, J. L., Rivas, M., Rodionova, V., Canepa, F., and Peddis, D., "A do-it-yourself approach for developing a magnetic field mapping setup using a 3D printer," *Measurement Science and Technology*, Vol. 34, No. 10, 2023. https://doi.org/10.1088/1361-6501/acde9b.

[18] Erglis, K., Cimurs, J., and Kitenbergs, G., "Low-Cost Solution for Magnetic Field Mapping Device," *2018 22nd International Conference Electronics*, 2018, pp. 1–5. https://doi.org/10.1109/ELECTRONICS.2018.8443648.

[19] Griffiths, D. J., *Introduction to Electrodynamics*, Pearson, 2013.